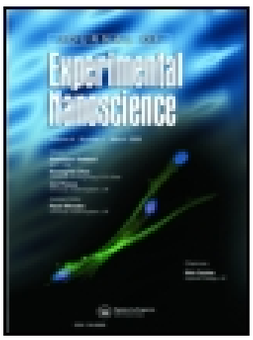

Journal of Experimental Nanoscience

ISSN: 1745-8080 (Print) 1745-8099 (Online) Journal homepage: http://www.tandfonline.com/loi/tjen20

Adhesion characteristics of Staphylococcus aureus bacterial cells on funnel-shaped palladium–cobalt alloy nanostructures

Junhua Gu, Paul Z. Chen, Brandon B. Seo, Joanna M. Jardin, Mohit S. Verma, Zeinab Jahed, Mohammad R. K. Mofrad, Frank X. Gu & Ting Y. Tsui

To cite this article: Junhua Gu, Paul Z. Chen, Brandon B. Seo, Joanna M. Jardin, Mohit S. Verma, Zeinab Jahed, Mohammad R. K. Mofrad, Frank X. Gu & Ting Y. Tsui (2015): Adhesion characteristics of Staphylococcus aureus bacterial cells on funnel-shaped palladium–cobalt alloy nanostructures, Journal of Experimental Nanoscience, DOI: 10.1080/17458080.2015.1083126

To link to this article: http://dx.doi.org/10.1080/17458080.2015.1083126

JOURNAL OF EXPERIMENTAL NANOSCIENCE, 2015
http://dx.doi.org/10.1080/17458080.2015.1083126

Taylor & Francis
Taylor & Francis Group

Adhesion characteristics of *Staphylococcus aureus* bacterial cells on funnel-shaped palladium−cobalt alloy nanostructures

Junhua Gu[a], Paul Z. Chen[a], Brandon B. Seo[c], Joanna M. Jardin[a], Mohit S. Verma[a], Zeinab Jahed[b], Mohammad R. K. Mofrad[b], Frank X. Gu[a] and Ting Y. Tsui[a,c]

[a]Department of Chemical Engineering, University of Waterloo, 200 University Avenue West, Waterloo, Canada; [b]Departments of Bioengineering and Mechanical Engineering, University of California Berkeley, Berkeley, CA, USA; [c]Department of Mechanical and Mechatronics Engineering, University of Waterloo, 200 University Avenue West, Waterloo, Canada

ABSTRACT

The adhesion properties of *Staphylococcus aureus* on palladium−cobalt (Pd−Co) alloy nanostructures with various cross-sectional geometries have been characterised. They include solid core, hollow, c-shaped, and x-shaped pillars. These pillars have unique funnel-shaped geometric features on the top surfaces with average included angles between ~142° and ~149°. The success rates of cell attachment on these pillar tops were quantified by using field emission scanning electron microscopy techniques. Results show the *Staphylococcus aureus* attachment rates of Pd−Co solid core, hollow, and x-shaped pillars are statistically indistinguishable with success rate up to 82%. X-shaped pillars have the lowest attachment rate among the four geometries of 46 ± 5%.

ARTICLE HISTORY
Received 25 March 2015
Accepted 9 August 2015

KEYWORDS
palladium; cobalt; nanopillar; *Staphylococcus aureus*; adhesion

1. Introduction

Staphylococcus aureus (*S. aureus*) is a micro-organism with grape-like shape generally smaller than 1000 nm while in suspension. They are often associated with post-surgical implant infections.[1−14] This is in part due to the strong affinity for these micro-organisms to adhere to a broad range of implant materials, such as stainless steel, titanium, and titanium alloys.[7,15−19] Once these bacterial cells attach on implant surfaces, they form colonies and are very difficult to remove. These surface-adhered micro-organisms multiply, grow biofilms, and subsequently cause infection in the patient.[3] While antibiotic medication can be used to control these infections, excessive and continuous usage of antibiotics may significantly increase the potential for the development of drug resistant strains of bacteria, such as methicillin-resistant *Staphylococcus aureus*.[6,18,20] Therefore, a drug-free approach is needed to reduce *S. aureus* cell adhesion on metal implant surfaces. One possible approach to reduce surface adhesion is through surface topography and architecture engineering. The effects of surface roughness or topography on cell adhesion have been characterised by numerous researchers and play an important role in controlling cell attachment.[15,17,18,21−27] The majority of these works were focused on the effects of bulk scale surface modification and treatment methods on bacterial cell adhesion and growth properties.[15,17,18,28] Recently, Jahed et al. [21] conducted an investigation to understand how individual *S. aureus* cells attach on electroplated nanocrystalline nickel nanopillar structures with various cross-sectional geometries − solid

CONTACT Frank X. Gu frank.gu@uwaterloo.ca; Ting Y. Tsui tttsui@uwaterloo.ca

core, hollow cylinder, c-shaped, and x-shaped. This report observed that there is indeed a causative relationship between the geometries and the cell attachment success rates on the nanopillar top surfaces. The reported results show significantly more *S. aureus* cells attached on c-shaped cylinder top surfaces than those with solid core and x-shaped structures. In addition, the observations suggest that a surface depression or via-hole in the centre of the nanopillar top surfaces may enhance cell adhesion behaviours.

The goal of this work is to test how nanometer scale architectures on palladium−cobalt (Pd−Co) alloy pillar top surfaces affect the adhesion characteristics of individual *S. aureus* cells. Unlike the nickel pillars manufactured by Jahed et al.,[21] where the top surfaces are smooth and flat, the Pd−Co alloy pillars fabricated for this work contain well-defined nanometer scale funnel-shaped surface depressions. Four different columnar features were fabricated with these funnel-shaped tops. They include solid core, hollow, c-shaped, and x-shaped pillars. This is believed to be the first demonstration of fabricating funnel-shaped Pd−Co pillars, and an original work in understanding how nanometer scale surface depressions affect individual *S. aureus* cell adhesion characteristics. Palladium alloy was selected for this work because palladium and its alloys have been used in implants.[29−31] In addition, recent work has demonstrated that gold-palladium coatings on polypropylene mesh graft implants and stainless steel substrates reduce post-surgical infection rates [32] and enhance long-term adhesion of human osteoblasts,[33] respectively. Several palladium (II) complexes recently developed also reveal their anti-bacterial characteristics.[34−37] Budige et al. [38] and Geeta et al. [39] evaluated the antibacterial activity of mononuclear Co(II), Ni(II), Cu(II), and Pd(II) complexes against multiple biological agents − *Bacillus subtilis, Staphylococcus aureus, Escherichia coli,* and *Klebsiella pneumonia*. They reported that Pd(II) complexes exhibited the most potent activity against these bacterial cells. Metallic form of Pd nanoparticles have also been demonstrated to be toxic to *Staphylococcus aureus*.[40]

Herein, the *S. aureus* bacterial cell adhesion behaviours on more than 800 Pd−Co funnel-shaped pillars were characterised. Results show Pd−Co pillars with solid core, hollow, and c-shaped structures perform indistinguishably and have the largest cell attachment success rates while the x-shaped pillars had much lower cell attachment success rates. The engineered funnel architectures appear to improve the adhesion characteristics of *S. aureus* bacterial cells on pillars with solid cores cross-sectional geometries.

2. Material and methods

2.1. Nanometer scale pillar fabrication

Palladium−cobalt alloy (Pd−Co) pillars were fabricated using electron beam lithography and electroplating techniques.[21,41] These nanostructures were prepared on silicon substrates coated with ~25 nm titanium thin films followed by a ~75 nm titanium tungsten alloy seed layer. After spin-coating the substrates with poly(methyl methacrylate) (PMMA) resists, arrays of via-hole patterns were created by using a Vistec EBPG 5000+ Electron Beam System and electron beam lithographic processes. The electron beam column was operating with an accelerating voltage of 100 kV. A commercially available plating solution manufactured by Technology without Limits (West Warwick, RI, USA) was used to deposit the Pd−Co metal in the via-holes. This electrolyte contains less than 1% tetra-ammine palladium (II) dichloride, less than 1% of cobalt, 2%−5% ammonium chloride, and less than 0.2% of ammonia. A platinised titanium mesh was used as anode. The deposition was carried out at ambient conditions with a direct current density of 13 ± 1.5 mA cm^{-2}. After the electroplating processes, excess PMMA were stripped by using acetone. Staedtler non-permanent markings were labelled on the substrates to help identifying Pd−Co specimens and pillar array locations during the cell deposition process. X-ray photoelectron spectroscopy analysis revealed the

electrodeposited blanket Pd−Co films compose of ∼49 atomic percentage of palladium and ∼51 atomic percentage of cobalt.

2.2. Cell culture

Staphylococcus aureus (ATCC 6538) bacterial cells were prepared in aseptic conditions. BD Biosciences trypicase soy agar was used to inoculate *S. aureus* bacterial cells at 37 °C for 24 hours. An amount of 5 mL of sterilised 2.55% saline with ∼0.006% nutrient broth added and calcium alginate swabs were used to harvest the bacterial cells into sterile 15 mL centrifuge tubes. The bacterial cells were then washed seven times through centrifugation at 4000 rpm for 10 minutes. After this, the suspensions were spectrophotometrically adjusted to an optical density of 1.33 at 600 nm. The plate counting method was employed to determine this concentration to be 10^9 CFU/mL. The prepared live *S. aureus* bacterial cell suspension was deposited on chips containing the Pd−Co pillar array. The chips were then loosely sealed within a plastic capsule to prevent significant evaporation and incubated at 37 °C for an hour. Afterwards, the chip surface was washed with deionised water to dislodge cells not well adhered. Finally, the chips were dried at 37 °C for at least 8 hours. The cell adhesion success rate is defined as the number of pillars with *S. aureus* cells remaining attached to the top surface of a specific cross-sectional geometry to the total counted number of pillars of the same geometry inspected.

2.3. SEM inspections

All of the specimens were inspected before and after the bacterial cell exposures using a high-resolution field emission scanning electron microscope (Zeiss LEO 1550). The electron gun was operating at an accelerating voltage of 10 kV with chamber pressure below 1.5×10^{-5} mbar. No gold coatings on the specimens were necessary and they were imaged as-received.

3. Results and discussion

3.1. Nanopillar geometries and surface architectures

More than 800 palladium−cobalt alloy (Pd−Co) pillars were fabricated and inspected for this work. Representative field emission scanning electron microscopy (FESEM) micrographs of Pd−Co pillars are displayed in Figure 1(a)−(i). These pillar stems have four cross-sectional geometries as shown in Figure 1(a)−(d); they include variations of solid core, hollow, c-shaped, and x-shaped pillars. These pillars were assembled in square arrays with a spacing of 10 μm as revealed in Figure 1(i). The physical characteristics and geometric dimensions of these specimens are summarised in Table 1. Figure 1(j) illustrates some of the pillar geometric parameters listed in this table. Since the Pd−Co deposition rates are fastest at the pillar outer edges, these pillars have funnel-shaped tops with sharp outer rim edges. This is uniquely different from the nickel pillars tested in our previous work [22] where the top surfaces are flat and even. Table 1 shows the average included angles of these funnel top features are in the range of approximately 142°− 149 °. The two pillars shown in Figure 1(a) and 1(b) consist of axisymmetric cone-like funnel tops with closed (solid core-shaped) and opened bottoms (hollow-shaped), respectively. The average depth of the funnel features on the solid core pillars is ∼145 nm. Figure 1(c) shows a micrograph of c-shaped pillar and it revealed a vertical slit opening along the pillar sidewall. It is important to note that the hollow-shaped pillars have their average inner diameter significantly larger than the c-shaped pillars of 696 ± 14 nm and 509 ± 14 nm, respectively. A micrograph of x-shaped pillar with four-fold symmetric funnel-shaped top surface is displayed in Figure 1(d). As the Pd−Co pillars continue to grow beyond its PMMA mould thickness, small mushroom-shaped caps begin to form as shown in Figure 1(e)−(h). The micrographs reveal these mushroom-shaped materials change the pillar surface topography. For example,

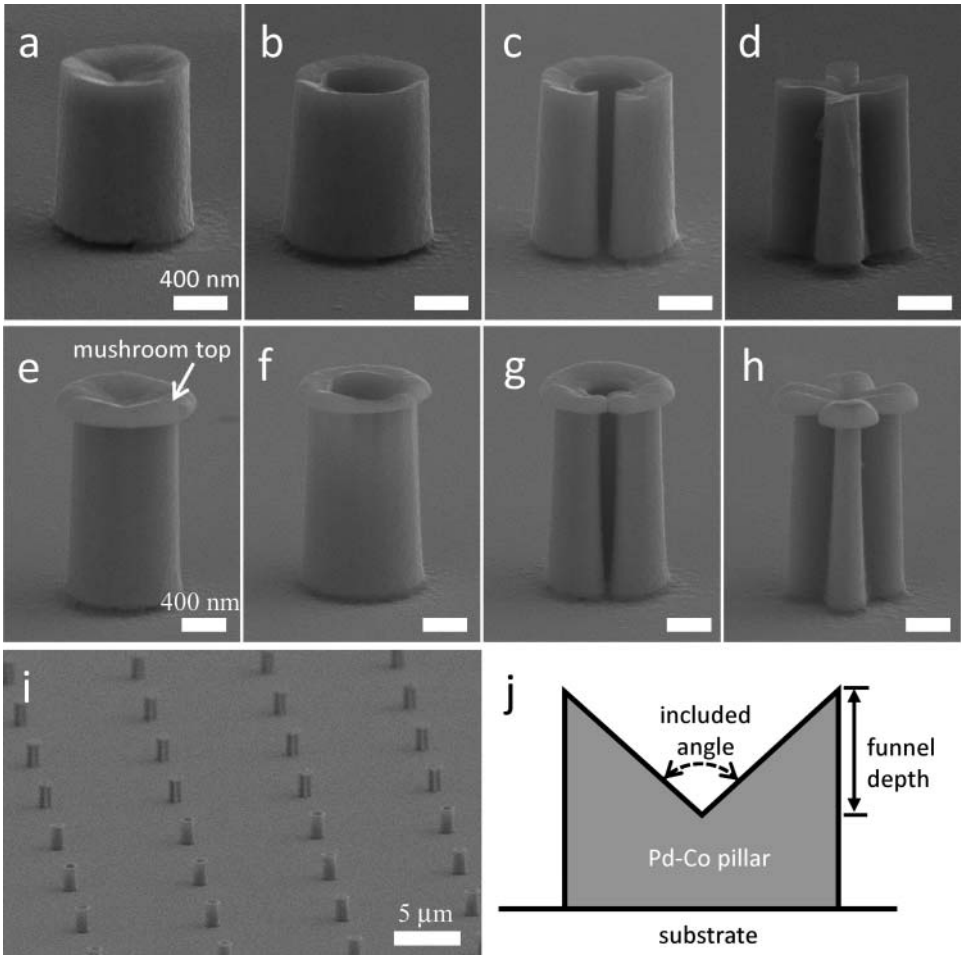

Figure 1. Typical SEM micrographs of as-fabricated palladium−cobalt nanopillars with (a) solid-core, (b) hollow, (c) c-shaped, and (d) x-shaped geometries. Pillars with small mushroom caps are displayed in (e)−(h). (i) Shows a low magnification micrograph displaying an array of nanopillars. Scale bars in (a)−(h) represents 400 nm while (i) bar corresponds to 5 μm. Schematic drawing of a solid pillar indicating geometric parameters is shown in (j).

the average inner diameters of the c-shaped pillars were reduced to 359 ± 16 nm. The average included angles of the hollow-shaped and c-shaped specimens increased by ~8°−15°, i.e. the funnel-shaped pillar tops with these two geometries flattened. Furthermore, the sharp outer rim edges became rounded with the formation of mushroom domes.

Table 1. Nanopillar geometric dimensions and *S. aureus* cell attachment rates on Pd−Co and nickel specimens. The data spreads correspond to one standard error. Values highlighted with curve brackets correspond to the number of nanopillars inspected.

	Pd−Co pillars without mushroom tops			Pd−Co pillars with mushroom tops			Nickel pillars	
Cross-sectional geometry	Cell attachment rates	Inner diameters (nm)	Included angles	Cell attachment rates	Inner diameters (nm)	Included angles	Cell attachment rates	Inner diameters (nm)
Hollow	81 ± 4% (102)	696 ± 14	143° ± 3°	66 ± 5% (104)	714 ± 12	168° ± 3°	83 ± 4% (113)	637 ± 17
C-shaped	82 ± 4% (106)	509 ± 14	142° ± 5°	47 ± 5% (108)	359 ± 16	150° ± 3°	56 ± 5% (105)	502 ± 13
Solid core	76 ± 4% (102)		145° ± 6°	43 ± 5% (98)		148° ± 5°	25 ± 4% (104)	
X-shaped	46 ± 5% (96)		149° ± 5°	35 ± 5% (96)		150° ± 4°	7 ± 2% (140)	

3.2. Staphylococcus aureus *adhesion characteristics on pillars without mushroom tops*

After exposing the funnel-shaped Pd−Co pillars to the *S. aureus* bacterial cells, inspection using FESEM techniques was performed. Typical micrographs of these pillars with bacterial cells are displayed in Figure 2(a)−(d). These structures do not contain mushroom tops. Visual inspections confirmed that *S. aureus* cells adhered on the top surfaces of the solid core, c-shaped, and x-shaped pillars. The change in the expected curvature at the bottom of the cells from grape-like to an impressed frame further validates the adhesion of the bacterial cells to respective pillars. In contrast, the bacterial cells fell into the interior openings of the hollow pillars, which are visible only in the top-down view of the pillars as shown in the inset of Figure 2(b) and supplementary Figures S1 and S2. The success rates for the bacterial cells to attach on pillars with different cross-sectional geometries were quantified and summarised in Table 1 and Figure 3. The number of pillars inspected for each geometric group is also included in the table and highlighted with curve brackets adjacent to the attachment rates. The data show *S. aureus* attachment rates of the axisymmetric pillars (hollow, c-shaped pillars, and solid core) are 81 ± 4%, 82 ± 4%, and 76 ± 4%, respectively. The data spread

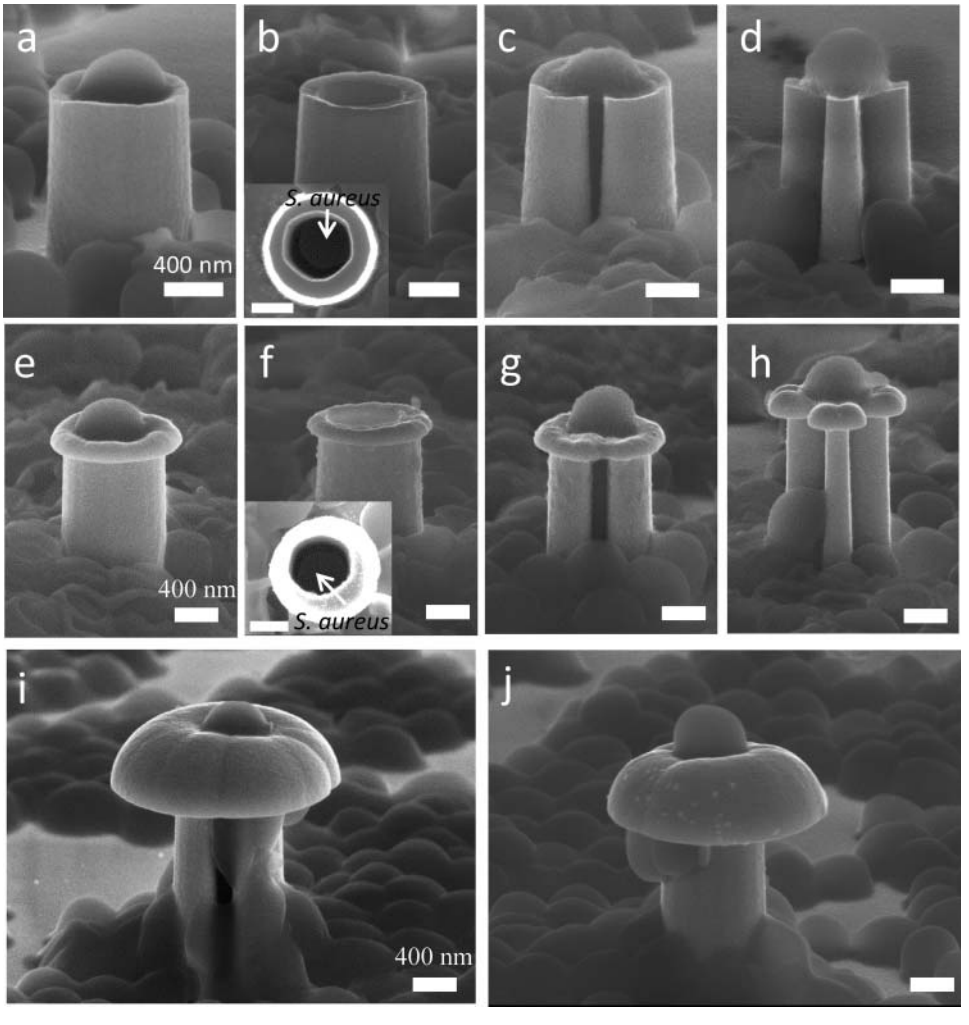

Figure 2. Typical SEM micrographs of the palladium−cobalt nanopillars exposed to *S. aureus*: (a) solid-core, (b) hollow, (c) c-shaped, and (d) x-shaped geometries. Pillars with small mushroom caps are displayed in (e)−(h). Inset images included in (b) and (f) are top-down views of the corresponding nanopillars. Scale bars represent 400 nm.

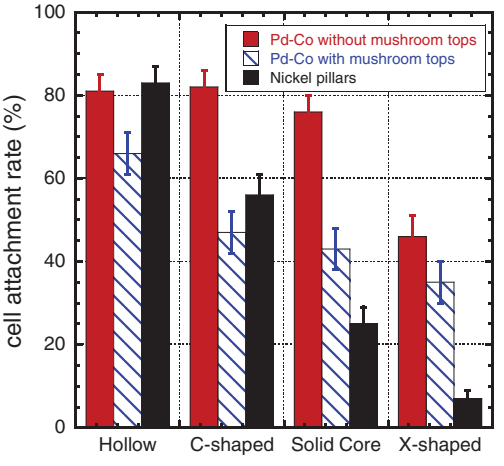

Figure 3. Plot of cell attachment rates as a function of pillar materials and cross-sectional geometries.

corresponds to one standard error. Results reveal the cell attachment rates of these three groups of specimens are statistically the same. The least efficient cross-sectional geometry is the x-shaped Pd−Co pillar with only 46 ± 5% of the sampled pillars covered with *S. aureus* cells.

As a comparison, identical cell type and concentrations were deposited on 462 nickel pillars fabricated with the same procedures and geometries described in the previous study.[22] Typical SEM micrographs of these nickel pillars are displayed in the Supplementary Figure S3. Unlike the funnel-shaped Pd−Co specimens, the nickel pillar tops are smooth and flat. It is important to note that different experimental parameters are being used during these cell adhesion experiments, such as dissimilar pillar materials (Pd−Co vs. Ni) and the seed layers (tungsten vs. gold). The attachment success rates of nickel pillars were also characterised. Visual inspections show all *S. aureus* cells rested within the interior openings of the hollow nickel pillars. In contrast, cells were attached on the top surface of solid core and x-shaped nickel pillars. Out of 105 c-shaped pillars with *S. aureus* attached, only two pillars observed to have cells resided in the interior while the remainder of these specimens have cells bonded on the top surfaces. These cell adhesion behaviours are similar to those observed in the Pd−Co specimens. Table 1 and Figure 3 revealed *S. aureus* cells attached on the nickel hollow pillars with success rates of 83 ± 4%, which are statistically indistinguishable from the Pd−Co counterparts consisting of cone-like funnel-shaped architectures of 81 ± 4%. It is remarkable that these two sets of specimens behave the same when considering different experimental parameters, such as various pillar metals and dissimilar seed layers. The only commonality among these specimens is the presence of similar diameter via-holes at the centre of these pillars, suggesting the significance of via-holes in nanometer scale pillars. In both cases, cells resided in the interior of these hollow pillars which protected them from being washed away during the rinsing process.

For c-shaped, solid core, and x-shaped nickel specimens, Table 1 and Figure 3 show cell attachment rates of 56 ± 5%, 25 ± 4%, and 7 ± 2%, respectively, which are significantly lower than the Pd−Co pillars with funnel-shaped tops of 82 ± 4%, 76 ± 4%, and 46 ± 5%, respectively. For both metals, the x-shaped specimens are the least favourable geometry for *S. aureus* cell attachment. It is not immediately clear if different bacterial fouling characteristics between Pd−Co and Ni, surface charge potential differences between the metals, or the funnel-shaped architecture in the Pd−Co pillars produce more favourable conditions for *S. aureus* to attach on these Pd−Co specimens. However, the different performances between solid-core and the c-shaped structures of the two metals suggest that the funnel-shaped top may be at least partly responsible for the increases of cell bonding on the solid core Pd−Co pillars. For Ni pillars, the c-shaped structures have average cell attachment rates at least two times larger than the solid core counterparts (56% vs. 25%). In contrast, the

attachment rates for the Pd−Co pillars of these two geometries show statistically insignificant differences (82 ± 4% vs. 76 ± 4%). It is unlikely that biofouling or surface charge differences between the two metals alone can account for the change of the geometric cell attachment dependence. This suggested that the success rates for *S. aureus* to be secured on the Pd−Co solid core pillar tops may be enhanced by other parameters, such as the funnel-shaped architectures.

3.3. Effects of mushroom-shaped pillar tops on cell adhesion

The *S. aureus* adhesion characteristics of small mushroom dome capped Pd−Co pillars are displayed in Figure 2(e)−(h). These specimens have small mushroom-shaped tops produced by slightly over-plating the pillar beyond the PMMA mould thickness. The micrographs show bacterial cells attached on the top surfaces of solid, c-shaped, and x-shaped pillars. For the hollow pillars, cells entered the interior of the pillars as revealed in the inset of Figure 2(f). Quantitative analysis of the cell attachment rates on the mushroom-capped pillars are summarised in Table 1 and Figure 3. Results show, regardless of the pillar cross-sectional geometries, *S. aureus* cells have difficulty securely bonding to these mushroom-shaped pillars. The attachment rates decline for pillars with all cross-sectional geometries. For example, the reduction is significant for c-shaped mushroom pillars with its success rate plunging to 47%. By rate, this decline represents a ∼43% reduction of cell bonding efficiently on these structures. Such poor ability for mushroom-shaped Pd−Co pillars to retain cells on their top surfaces may be in part due to the 29% shrinkage of the average via-hole diameters caused by the formation of the mushroom caps. In addition, as the mushroom caps grew, the average funnel included angles increase as shown in Table 1 and thus the c-shaped pillar tops are flattened. This removes the protection created by the funnel-shaped features from the environment. Furthermore, the formation of mushroom features smooth out the pillar sharp rim edges. It is unclear if or how this geometric change affects the cell attachment behaviours.

Specimens with large Pd−Co mushroom domes were also fabricated and exposed to *S. aureus* cells as displayed in Figure 2(i) and 2(j). These mushrooms were formed by lengthening the deposition time and they consist of a surface depression at the centre of the structure. The dome heights are ∼800 nm. These micrographs show *S. aureus* cells have the ability to bind on the mushroom surface depressions and the bottom surfaces of the mushroom caps. In addition, micrographs show these bacterial cells bonded to Pd−Co pillars do not bend or mechanically deform the respective pillars. This is in contrast with the previous work [22] where majority of 220 nm diameter nickel mushroom-shaped pillars bend downward after *S. aureus* cells attached to the pillars. This is most likely because the Pd−Co pillar diameter is ∼1000 nm − about five times larger and much stiffer than the nickel specimens tested previously. Thus, these structures are considerably more stable than their thinner nickel counterparts in the presence of bacterial adhesions.

It is important to note that the cell attachment results summarised in Figure 3 may vary with the cell concentration in the deposition solution. This concentration dependence is expected to be affected by the pillar geometries which govern the cell attachment mechanisms. When the *S. aureus* concentration in the deposition solution increases, it is expected that more cells will successfully attach on the pillars regardless of their geometry. However, the rate of increase may be sensitive to the pillar shapes. For instance, *S. aureus* cells entered the interior of the hollow pillars are well protected from being removed by external forces. The attachment rate-limiting factor for this geometry is the probability that cells entered the via-holes. Other rate-determining parameters, such as the resident time needed for the adhesion bonds to form with the metal, are less significant as the deep via holes prevent the micro-organisms from escaping. In contrast, the attachment rates of solid core samples will not only depend on the probability that the cells rest on the top surfaces but also the resident time cells required to form chemical adhesion bonds with the pillar. Therefore, cell attachment rate relationships among various pillar geometries as shown in Figure 3 may change with cell concentrations in the cell deposition solution.

Evidences presented in this work reveal the interplay between distinct pillar funnel-shaped tops, mushroom caps, and cross-sectional geometries in the successful adhesion of S. aureus bacterial cells. Results show these well-defined surface architectures may affect the adhesion of *S. aureus* on metallic surfaces in a complex manner. The results suggest that common practices attempting to relate the cell adhesion behaviours with surface finishing methods by using ordinary surface roughness parameters, such as root-mean-squared (rms) surface roughness, may not be sufficient, since the surface architectural geometric parameters are not defined.

4. Conclusions

The adhesion properties of *S. aureus* on Pd−Co pillars with funnel-shaped surface features have been characterised and their results were compared with nanocrystalline nickel pillars. Results show that hollow pillar structures are the best geometries to promote cell adhesion in both Pd−Co and Ni structures while x-shaped pillars performs the worst. In contrast, the funnel-shaped architectures may aid *S. aureus* in bonding to the top surfaces of solid core pillars. Finally, the mushroom top cap of the pillar degrades the attachment rates of *S. aureus*. This demonstrates that surface depression in the nanometer scale with large included angles is a critical parameter that influences *S. aureus* cell surface adhesion behaviours.

Acknowledgments

One of the author, Ting YiuTsui, would like to thank Natural Sciences and Engineering Research Council of Canada (NSERC) Discovery grant RGPIN-355552 and RTI grant [EQPEQ-391005] for the support of this work. Junhua Gu would like to thank Soochow University, China, and China Scholarship Council for his scholarship supports.

Disclosure statement

No potential conflict of interest was reported by the authors.

Funding

Ting YiuTsui: Natural Sciences and Engineering Research Council of Canada (NSERC) [Discovery grant number RGPIN-355552], [RTI grant number EQPEQ-391005].

Supplemental data

Supplemental data for this article can be accessed here.

References

[1] Chiu H-C, Lee S-L, Kapuriya N, et al. Development of novel antibacterial agents against methicillin-resistant *Staphylococcus aureus*. Bioorg Med Chem. 2012;20(15):4653−4660.
[2] Cordero J, Munuera L, Folgueira MD, Influence of metal implants on infection − an experimental study in rabbits. J Bone Jt Surg [British]. 1994;76(5):717−720.
[3] Gristina AG. Biomaterial-centered adhesion versus infection : microbial tissue integration. Science. 1987;237 (4822):1588−1595.
[4] Gross M, Cramton SE, Go F, et al. Key role of teichoic acid net charge in *Staphylococcus aureus* colonization of artificial surfaces. Infect Immun. 2001;69(5):3423−3426.
[5] Harris LG, Tosatti S, Wieland M, et al. *Staphylococcus aureus* adhesion to titanium oxide surfaces coated with non-functionalized and peptide-functionalized poly(L-lysine)-grafted-poly(ethylene glycol) copolymers. Biomaterials. 2004;25(18):4135−4148.
[6] Holden MTG, Feil EJ, Lindsay Ja, et al. Complete genomes of two clinical *Staphylococcus aureus* strains: evidence for the rapid evolution of virulence and drug resistance. Proc Natl Acad Sci USA. 2004;101(26):9786−9791.

[7] Melcher GA, Printzen G, Schlegel U, et al. Infection after intramedullary investigation on rabbits nailing: an experimental investigation on rabbits. Injury. 1996;27(3):23–26.
[8] Moran E, Byren I, Atkins BL. The diagnosis and management of prosthetic joint infections. J Antimicrob Chemother. 2010;65(Suppl 3):iii45–iii54.
[9] Oga M, Sugioka Y, Hobgood CD, et al. Surgical biomaterials and differential colonization by Staphylococcus epidermidis. Biomaterials. 1988;9(3):285–289.
[10] Rochford ETJ, Poulsson AHC, Salavarrieta Varela J, et al. Bacterial adhesion to orthopaedic implant materials and a novel oxygen plasma modified PEEK surface. Colloids Surf B Biointerfaces. 2014;113:213–222.
[11] Teterycz D, Ferry T, Lew D, et al. Outcome of orthopedic implant infections due to different staphylococci. Int J Infect Dis. 2010;14(10):e913–e918.
[12] Wang X, Wang G, Liang J, et al. *Staphylococcus aureus* adhesion to different implant surface coatings: an *in vitro* study. Surf Coat Technol. 2009;203(22):3454–3458.
[13] Qian S, Qiao Y, Liu X. Selective biofunctional modification of titanium implants for osteogenic and antibacterial. J Mater Chem B Mater Biol Med. 2014;2:7475–7487.
[14] Gristina AG, Hobgood CD, Webb LX, et al. Adhesive colonization of biomaterials and antibiotic resistance. Biomaterials. 1987;8(6):423–426.
[15] Harris LG, Richards RG. Staphylococci and implant surfaces: a review. Injury. 2006;37(Suppl 2):S3–S14.
[16] Barth E, Myrvik QM, Wagner W, et al. *In vitro* and *in vivo* comparative colonization of Staphylococcus aureus and Staphylococcus epidermidis on orthopaedic implant materials. Biomaterials. 1989;10:325–328.
[17] Crawford RJ, Webb HK, Truong VK, et al. Surface topographical factors influencing bacterial attachment. Adv Colloid Interface Sci. 2012;179–182:142–149.
[18] Harris LG, Meredith DO, Eschbach L, et al. *Staphylococcus aureus* adhesion to standard micro-rough and electropolished implant materials. J Mater Sci Mater Med. 2007;18(6):1151–1156.
[19] Hu X, Neoh K-G, Shi Z, et al. An *in vitro* assessment of titanium functionalized with polysaccharides conjugated with vascular endothelial growth factor for enhanced osseointegration and inhibition of bacterial adhesion. Biomaterials. 2010;31(34):8854–8863.
[20] Karska-Wysocki B, Bazo M, Smoragiewicz W. Antibacterial activity of Lactobacillus acidophilus and Lactobacillus casei against methicillin-resistant *Staphylococcus aureus* (MRSA). Microbiol Res. 2010; 165(8):674–686.
[21] Jahed Z, Lin P, Seo BB, et al. Responses of *Staphylococcus aureus* bacterial cells to nanocrystalline nickel nanostructures. Biomaterials. 2014;35(14):4249–4254.
[22] Nill P, Goehring N, Loeffler R, et al. Studying bacterial adhesion forces: *Staphylococcus aureus* on elastic poly (dimethyl)siloxane substrates. Microelectron Eng. 2011;88(8):1825–1827.
[23] Özçelik H, Padeste C, Hasirci V. Systematically organized nanopillar arrays reveal differences in adhesion and alignment properties of BMSC and Saos-2 cells. Colloids Surf B Biointerfaces. 2014;119:71–81.
[24] Puckett SD, Taylor E, Raimondo T, et al. The relationship between the nanostructure of titanium surfaces and bacterial attachment. Biomaterials. 2010;31(4):706–713.
[25] Wu Y, Zitelli JP, TenHuisen KS, et al. Differential response of Staphylococci and osteoblasts to varying titanium surface roughness. Biomaterials. 2011;32(4):951–960.
[26] Zink C, Hall H, Brunette DM, et al. Orthogonal nanometer-micrometer roughness gradients probe morphological influences on cell behavior. Biomaterials. 2012;33(32):8055–8061.
[27] Izquierdo-Barba I, García-Martín JM, Álvarez R, et al. Nanocolumnar coatings with selective behavior towards osteoblast and *Staphylococcus aureus* proliferation. Acta Biomater. 2015;15:20–28.
[28] Truong VK, Lapovok R, Estrin YS, et al. The influence of nano-scale surface roughness on bacterial adhesion to ultrafine-grained titanium. Biomaterials. 2010;31(13):3674–3683.
[29] Paulus J, Parida GR, Tucker RD, et al. Corrosion analysis of NiCu and PdCo thermal seed alloys used as interstitial hyperthermia implants. Biomaterials. 1997;18(24):1609–1614.
[30] Vergos VK, Papadopoulos TD. Characterization of the interface of two dental palladium alloys cast on a prefabricated implant gold cylinder. J Alloys Compd. 2009;478(1–2):863–867.
[31] Wataha JC, Lockwood PE, Regina LW, et al. Brushing-induced surface roughness of dental casting alloys. J Prosthet Dent. 2008;99(6):455–460.
[32] Saygun O, Agalar C, Aydinuraz K, et al. Gold and gold-palladium coated polypropylene grafts in a S. epidermidis wound infection model. J Surg Res. 2006;131(1):73–79.
[33] Anselme K, Bigerelle M. Effect of a gold–palladium coating on the long-term adhesion of human osteoblasts on biocompatible metallic materials. Surf Coatings Technol. 2006;200(22–23):6325–6330.
[34] Özdemir ÜÖ, Akkaya N, Özbek N. New nickel(II), palladium(II), platinum(II) complexes with aromatic methanesulfonylhydrazone based ligands. Synthesis, spectroscopic characterization and *in vitro* antibacterial evaluation. Inorganica Chim Acta. 2013;400:13–19.

[35] Prasad KS, Kumar LS, Chandan S, et al. Palladium(II) complexes as biologically potent metallo-drugs: synthesis, spectral characterization, DNA interaction studies and antibacterial activity. Spectrochim Acta A Mol Biomol Spectrosc. 2013;107:108–116.
[36] Patel MN, Patidar AP, Karia PS, et al. Cytotoxic, antibacterial and nucleic acid interaction studies of square planar palladium(II) complexes. Inorganica Chim Acta. 2014;419:45–54.
[37] Akbar Ali M, Mirza AH, Butcher RJ, et al. Biological activity of palladium(II) and platinum(II) complexes of the acetone Schiff bases of S-methyl- and S-benzyldithiocarbazate and the X-ray crystal structure of the [Pd(asme)2] (asme = anionic form of the acetone Schiff base of S-methyldithiocarbazat. J Inorg Biochem. 2002; 92(3–4):141–148.
[38] Budige G, Puchakayala MR, Kongara SR, et al. Synthesis, characterization and biological evaluation of mononuclear Co (II), Ni (II), Cu (II) and Pd (II) complexes with new N_2 O_2 Schiff base ligands. Chem Pharm Bull. 2011;59(2):166–171.
[39] Geeta B, Shravankumar K, Reddy PM, et al. Binuclear cobalt(II), nickel(II), copper(II) and palladium(II) complexes of a new Schiff-base as ligand: synthesis, structural characterization, and antibacterial activity. Spectrochim Acta A Mol Biomol Spectrosc. 2010;77(4):911–915.
[40] Adams CP, Walker KA, Obare SO, et al. Size-dependent antimicrobial effects of novel palladium nanoparticles. PLoS One. 2014;9(1):e85981.
[41] Burek MJ, Greer JR. Fabrication and microstructure control of nanoscale mechanical testing specimens via electron beam lithography and electroplating. Nano Lett. 2010;10(1):69–76.